Chalcogenide Letters Vol. 14, No. 6, June 2017, p. 227 - 237

n-TYPE IRON PYRITE (FeS_2) THIN-FILMS OBTAINED AT DIFFERENT SULFUR VAPOR PRESSURES

R. P. SRIVASTAVA, A. P. SAXENA, S. INGOLE*
Laboratory for Photovoltaic and Energy Storage Materials, Department of Materials Science and Engineering, Indian Institute of Technology, Kanpur-208016, India

Iron-pyrite (FeS_2) has received renewed interest for photovoltaic application due to its high absorption coefficient, abundant supply of constituent elements and expected environment friendliness. In the present investigation, thin-films of iron-pyrite were obtained via sulfurization of sol-gel synthesized hematite (Fe_2O_3) films at 550 °C and sulfur vapor pressures ranging from 30.4 kPa (0.3atm) to 319.2 kPa (3.15atm). For the studied sulfurization pressure range, each of the iron-pyrite thin-films showed n-type conductivity with charge carrier concentration decreasing by an order of magnitude (10^{21} to 10^{20} cm^{-3}). The corresponding change in the S/Fe ratio was from 1.81 to 1.99.

(Received May 30, 2017; Accepted June 20, 2017)

Keywords: Iron pyrite, thin-films, sulfurization, sulfur vapor pressure, AC field Hall measurement, Mott-Schottky

1. Introduction

Iron-pyrite (FeS_2), hereafter referred to as pyrite, has received renewed interest for photovoltaic (PV) application due to the abundant supply of the constituent elements iron and sulfur, expected environment friendliness, and high absorption coefficient ($> 5\times10^5$ cm^{-1} for wavelength $\lambda < 900$ nm) [1]. The theoretically estimated efficiency of a PV device using pyrite as a photoabsorber is 28 % [2]; however, the highest reported efficiency has so far remained 2.8% [3]. To better understand the structure – property correlation several investigations have been carried out on both the single crystals [4-13] and polycrystalline thin films of this material [14-30]. Among the several approaches reported, the majority have obtained thin-films of polycrystalline pyrite via sulfuirzation of precursor films in a sealed ampoule, where, thin-films of iron, iron-oxide, or certain compounds of iron and sulfur are treated with sulfur-vapor [31-40]. In this context, several research groups have reported the effect of sulfurization temperature and time on the electrical and optical properties of pyrite [41-51]. However, the reports on the influence of sulfur vapor pressure are few [52-55]; moreover, in these studies the pressure has been estimated based on certain simplifying assumptions such as ideal gas behavior, considering that sulfur vapor is comprised of single molecular species in spite of the fact that it could contain several species (S_n, $2 < n < 10$). Rau et al. have measured the sulfur vapor pressure versus vapor density at various temperatures which are in good agreement with the theoretically estimated values [56]. Their data should allow estimation of sulfurization pressure inside an ampoule with greater confidence. Therefore, in the present work this data has been implemented to obtain desired sulfurization pressures inside an ampoule and corresponding effects on the properties of pyrite have been reported. In the following discussion the term *pressure* will be used instead of the term *sulfurization pressure*.

---

*Corresponding author: sarang@iitk.ac.in

2. Experimental section

2.1. Materials

Analytical grade iron nitrate nonahydrate [$Fe(NO_3)_3.9H_2O$], absolute ethanol, propylene oxide (PO), and carbon disulfide were purchased from Alfa Aesar. Sulfur powder (99.998%) was purchased from Sigma Aldrich. All the chemicals were used as received.

2.2. Synthesis of precursor solution and thin-films

The thin-films of hematite (α-Fe_2O_3) were obtained onto quartz substrates through sol-gel route. For this purpose 6.4 mmol (2.59 g) iron nitrate nonahydrate was dissolved in 10 ml ethanol followed by addition of a fixed volume of propylene oxide. This precursor solution was maintained at 20 °C for 40 hours prior to spin coating of films onto quartz substrate. Spin coating was performed at 3000 rpm for 30 s and two consecutive layers were spin coated with intermediate drying at 400 °C. Prior to coating of films the substrates were cleaned in a mild soap solution followed by piranha (3:1 solution of H_2SO_4 and H_2O_2) cleaning.

2.3. Sulfurization of hematite thin-films

Sulfurization was performed at 550°C for 90 minutes in sealed quartz ampoules (Fig. 1). The pressures selected for the investigation were based on the data for the pressure versus sulfur vapor density reported by Rau et al. and the amount of sulfur powder used for obtaining these pressures have been shown in Table 1. Amount of sulfur powder corresponding to 30.4 kPa pressure was calculated with the given data and ampoule volume was determined. All of these pressures are lower than the saturation vapor pressure for sulfur at 550 °C which is 372.9 kPa [57]. The ampoules were purged with argon three times before sealing under the dynamic vacuum of 10^{-6} kPa. During sulfurization the tube furnace was heated at the rate of 2 °C/min while the cooling rate was kept at 1.5 °C/min. The heating and cooling rate were found to be very important for obtaining well adherent films. The offset between the furnace temperature as measured at the outer surface of the alumina tube and the temperature of the quartz substrate inside the sealed ampoule was taken into the consideration. Any possible pressure change due to the amount of sulfur consumed, by product gases released during Fe_2O_3 to FeS_2 transformation, and the volume expansion for the quartz tube at 550 °C has been considered to be negligible.

Table 1.Amount of sulfur powder placed inside an ampoule for achieving different sulfurization pressures

Pressure kPa (atm)	Amount of sulfur powder (milligram)
30.4 (0.300)	6.6
69.8 (0.689)	30.4
117.2 (1.157)	53.5
188.9 (1.864)	92.9
232.5 (2.295)	122.5
319.2 (3.150)	166.8

Fig. 1. Schematic of an ampoule containing a hematite thin-film coated quartz-substrate and sulfur powder.

2.4. Characterization

The structural characterization of thin-films was carried out at the PAN Analytical X-ray diffractometer equipped with CuKα radiation (λ = 1.54Å) with a scan rate of 2-seconds/step at a grazing angle of 1.5°. The X-ray source was set at 45kV and 40mA. The surface morphology and cross-sectional analysis was carried out with the help of JEOL (JSM-7100F) field emission scanning electron microscope (FE-SEM). The elemental composition was estimated using energy-dispersive analysis of X-ray (EDAX). Raman spectroscopy was carried out using 532 nm laser, 50X objective lens, and maximum incident power of 2mW with an integration time of 2 seconds using STR series Raman Spectrometer. The instrumental resolution was 3cm^{-1}. The optical absorption spectra were obtained using Carry 7000 Universal measurement spectrophotometer from Agilent technologies. The majority charge carrier type and density was obtained from AC field Hall effect measurement performed at Lake Shore Model 8404 AC/DC Hall Effect Measurement System. The Ohmic contacts with pyrite were obtained using silver paste. The chemical state of constituents and the presence of possible contaminants on the pyrite surface were detected by X-ray photoelectron spectroscopy (XPS) with PHI 5000 VersaProbe II form FEI Inc. Root-mean-square (RMS) roughness was measured using Asylum research atomic force microscope (AFM). Electrochemical measurements were done using a conventional three-electrode cell. Pyrite film deposited on the Molybdenum coated glass substrates were used as working electrode. A saturated calomel electrode (SCE) and a platinum counter electrode were used in the cell. All the electrode potentials reported in this study are referenced to SCE. Electrochemical measurement was done in deaerated pH 6.5 buffer solution at ambient temperate. Photocurrent measurements were performed under the AM1.5G illumination obtained from a class AAA, OAI TriSOL solar simulator.

3. Results and discussion

In Fig. 2, the plot ***a*** is an X-ray diffraction (XRD) pattern for the thin-film prior to sulfurization and plots ***b*** to ***g*** are for the thin-films obtained after sulfurization at different pressures. All the intensity peaks in plot ***a*** matches with the pattern in JCPDS file no. 33-0664 corresponding to rhombohedral α-Fe_2O_3 (Hematite), and those for the plots ***b*** to ***g*** match with the JCPDS file no. 42-1340 corresponding to cubic pyrite. The X-ray diffraction obtained from the synthesized pyrite films did not show any signal from impurity phases such as marcasite, iron monosulfide, pyrrhotite or iron oxides.

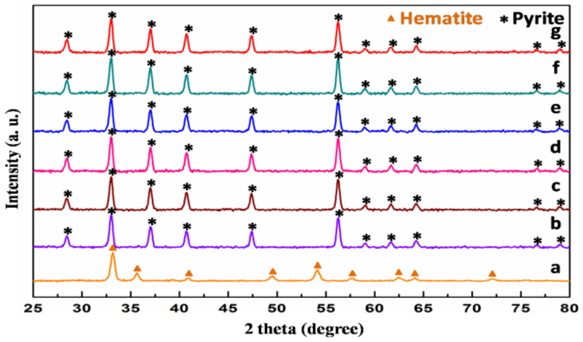

Fig. 2. XRD spectra for (a) hematite thin-film, (b) to (g) thin-films obtained after sulfurization of hematite films at 30.4, 69.8, 117.2, 188.9, 232.5, and 319.2 kPa, respectively.

The lattice parameters calculated from the XRD pattern (Fig. 2, plots ***b*** to ***g***) for all the pyrite films found to be in the range 5.428 – 5.414 Å for the polycrystalline thin films [58].Raman spectroscopy which is apparently more sensitive compared to XRD technique for the detection of trace amount of phases [59] was used in order to detect presence of secondary phases such as troilite (FeS) and marcasite (orthorhombic FeS_2) which are expected to deteriorate the performance of cubic pyrite in PV application [60]. In the Raman spectra [Fig. 3] plot ***a*** corresponding to the film prior to sulfurization has all the peaks corresponding to hematite. The plots ***b*** to ***g*** are corresponding to pyrite films obtained at different sulfurization pressures. The Raman spectra for the pyrite films showed three characteristic phonon modes at wavenumber 337 cm^{-1} (E_g), 372 cm^{-1} (A_g) and 424 cm^{-1} (T_g). The two modes E_g and A_g signify the presence of S-S bond in the pyrite sample [61]. The mode at 424 cm^{-1} caused by third Raman active mode and corresponds to coupled libration and stretching in the pyrite [62]. No secondary phases of iron and sulfur such as troilite (FeS), greigite (Fe_3S_4), mackinawite ($Fe_{1+x}S$), pyrrhotite ($Fe_{1-x}S$), marcasite and iron oxide were observed within the detection limit of the instruments. Both the XRD and Raman analysis of the films obtained at different sulfur vapor pressures confirmed the high phase purity or pyrite films without any secondary phase.

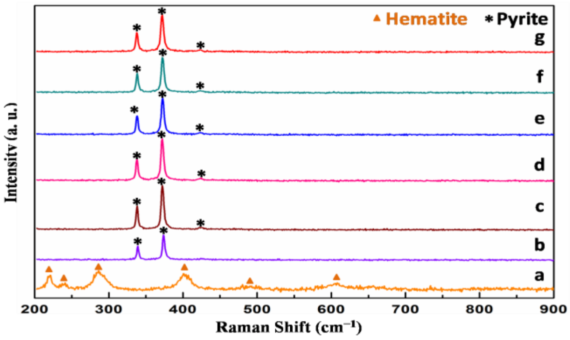

Fig. 3. Raman spectra for (a) hematite thin-film, (b) to (g) thin-films obtained after sulfurization of hematite films at 30.4, 69.8, 117.2, 188.9, 232.5, and 319.2 kPa, respectively

Further to confirm the binding states of the iron and sulfur in the sulfurized thin films X-ray photoelectron spectroscopy (XPS) is performed. Pyrite films corresponding to the lowest and highest sulfurization pressures were analyzed using this technique and the observations are shown in Fig. 4. Fe $2p_{3/2}$ and Fe $2p_{1/2}$ peaks have been observed at 707 eV and 719.7eV, respectively, in Fig.4(a1) and (b1), which are consistent with the binding energy of Fe in FeS_2[63].

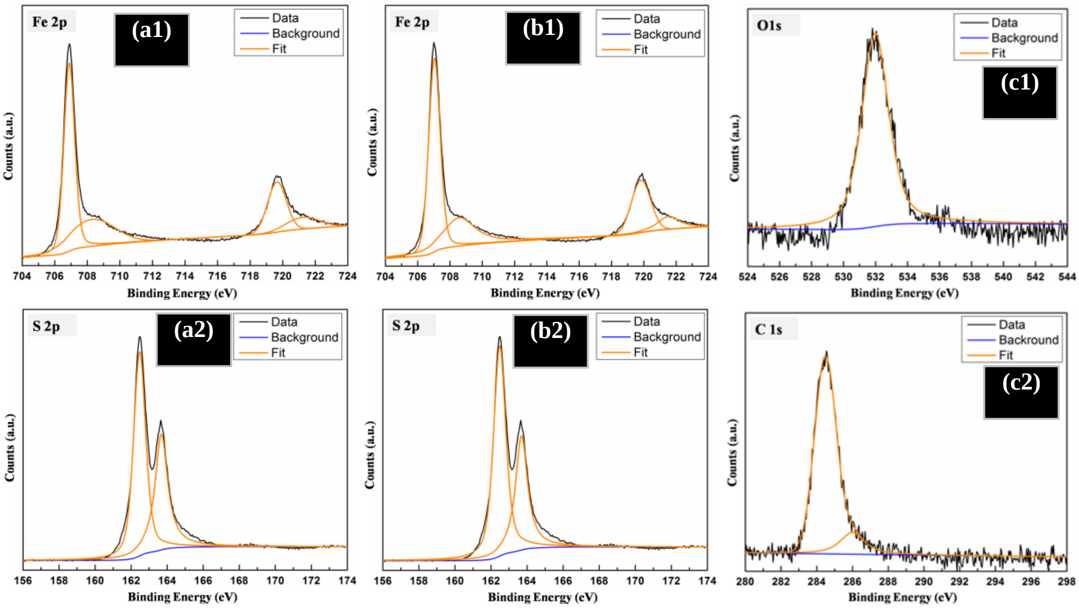

Fig. 4. XPS spectra of the films sulfurized at (a1-a2). 30.4 kPa (b1-b2) 319.2 kPa sulfurization pressures. (c1-c2) O 1s and C1s spectra for the pyrite films.

Both of these peaks also show energy tails (~ 708.4 eV and 721.2 eV) which have been attributed to the presence of sulfide or oxide compounds of Fe (III) on the surface [64]. The corresponding $S2p_{3/2}$ and $S2p_{1/2}$ peaks at 162.3 eV and 163.5 eV (Fig.4(a2) and (b2))are characteristic of S_2^{2-} in the pyrite [63]. There is no peak corresponding to binding energy 161 eV has been observed which is a characteristic of the S^{2-}[65]. The observed oxygen O1s signal at 532 eV for all the films may be due to the presence of hydroxide species on the surface [Fig.4(c1)]. This signal was not observed after sputtering few monolayers of the film. Smestad et al. have reported similar observations [36]. In Fig.4(c2), C1s spectra show two peaks at 284.5 eV (C-C) and 286±0.1 eV (C-O); this carbon presence may be due to the adsorption of adventitious hydrocarbons and alcohols onto the film surface. Similar observations have been made by Seefeld et al. [64, 66].

Fig.5(a) shows FESEM micrograph of a representative hematite film used for sulfurization. These films are continuous with micro-cracks on the surface, and the root-mean-square (RMS) roughness of less than 5 nm. Fig.5 (***b*** to ***g***) show the FESEM micrographs of the pyrite films obtained at increasing pressures. All are crystalline with grain size ranging from ~50 to few 100s of nanometers. The film corresponding to the lowest pressure is relatively compact with negligible pores while those corresponding to higher pressures have developed regions with loosely packed grains. Simultaneously, the films have developed large grains ≥200 nm) distributed in the background of relatively smaller grains (≤100 nm or smaller) with the increasing pressure. This could explain the observed increase in the RMS roughness of the films with the increasing sulfurization pressure (Fig. 6). The cross-sectional FESEM was done to obtain the thickness of pyrite films at different sulfurization pressures.

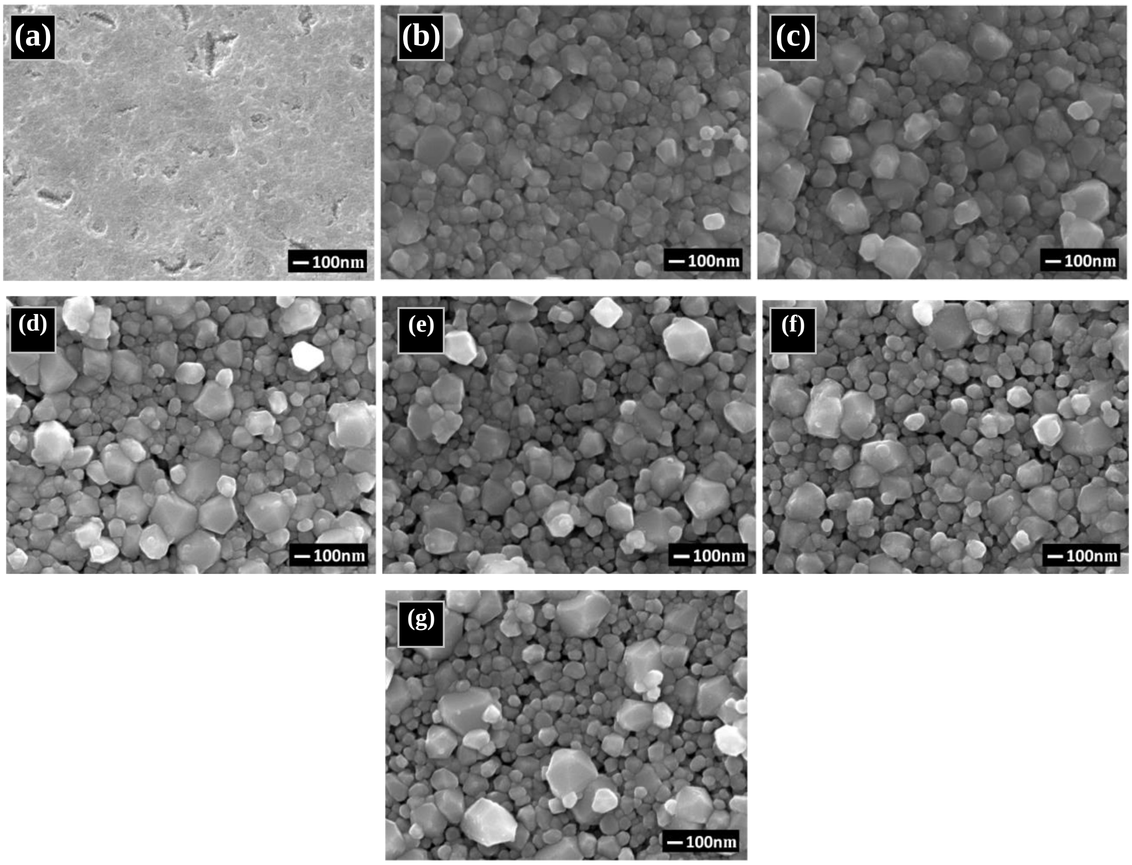

Fig. 5. Morphology of (a) as synthesized precursor thin-film, (b) to (g) precursor thin-films after sulfurization for 1.5 h at 30.4, 69.8, 117.2, 188.9, 232.5, and 319.2 kPa, respectively.

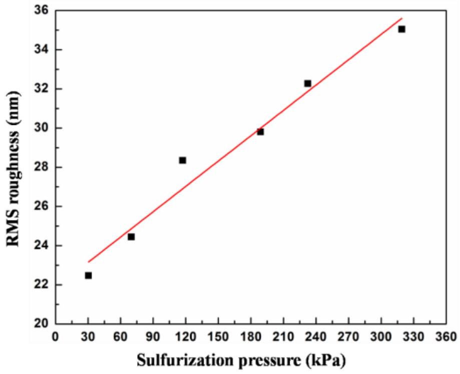

Fig. 6. RMS roughness of the pyrite films at different sulfurization pressures.

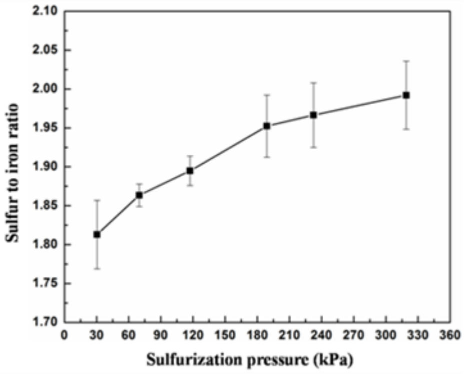

Fig. 7. Sulfur to iron ratio for the pyrite films at different sulfurization pressures

Fig. 7 shows S/Fe ratio obtained from as synthesized pyrite films. The S/Fe ratio has increased with sulfurization pressure and approached closer to the ideal value of 2. Considering the large energy (2.18 and 1.66 eV) required for the creation of V_{Fe} and V_S in pyrite, the corresponding S/Fe ratio is expected to lie in the range of $1.98 < S/Fe < 2.02$, only [67]. The films obtained at higher pressures are showing S/Fe ratio within this range, however, the films corresponding to the lower pressures have S/Fe ratio less than this range. Presence of sulfur poor phase or an unreacted Fe_2O_3 could account for this deviation observed in the S/Fe ratio, however, none of these were detected in the XRD and Raman analysis for any of the pyrite films. Another possibility could be incomplete removal of oxygen from film during its conversion to FeS_2. The possibility of homogeneously distributed oxygen is under investigation through TEM.

The Hall effect measurements performed using DC field were inconsistent. Several other groups have reported similar observations with the DC field Hall measurement on pyrite citing the low mobility of charge carriers [45,64] which prevented them to measure the type of the conductivity of the pyrite films. In our DC field measurement for the same film few of the repeated measurements indicated it to be n-type while for the other measurements the same film was indicated to be a p-type but all the measurements showed a very low mobility in the range of 10^{-1}-10^{-2}cm^{2}V^{-1}s^{-1}. The AC Hall technique is considered more reliable for the materials with low charge carrier mobility as compared to DC field Hall Effect measurement. Rettie et al. reported that they could not measure the mobility of molybdenum (Mo) and tungsten (W) doped bismuth vanadate ($BiVO_4$) with dc field hall measurement because of the low mobility of the material. Only ac filed hall measurement has provided a mobility value of 0.2 cm^{2}V^{-1}s^{-1}[68]. In the present case also the Hall mobility is very low therefore; AC field Hall measurement was performed on all the synthesized pyrite films. AC field Hall measurement consistently indicated all the films to be n-type and very low mobility value in the range of $1.74 - 6.22 \times 10^{-3}$ cm^{2}V^{-1}s^{-1} was obtained. This observation is in contrast to a large fraction of literature on synthesized pyrite films where the type of majority charge carriers has been reported to be holes as determined using DC field Hall effect measurement [24, 30, 40, 69, 70, 71]. Recently few other groups also have reported n-type conductivity in the synthesized pyrite films as determined using low noise AC measurement technique or electrochemical Mott-Schottky technique [45,51] The n-type conductivity has been observed primarily for the single crystal pyrite [7,10,12,72]. Charge carrier density and resistivity of the all the pyrite films determined using AC field Hall Effect measurement is shown in Fig. 8. The majority charge carrier concentration was found to be of the order of the 10^{21} cm^{-3} which is in agreement with the previous reports on the pyrite [50, 51]. From the Fig.8(a) it can be seen that the majority charge carrier concentration decreased by an order of magnitude for an order of magnitude increase in the sulfurization pressure. Since the S/Fe ratio increased with pressure [Fig. 7] the corresponding drop in the sulfur vacancy concentration is expected, and since sulfur vacancies act as donors [18] the observed drop in the charge carrier concentration is expected. It in turn has contributed towards the increase in the resistivity of pyrite films [Fig.8(b)].

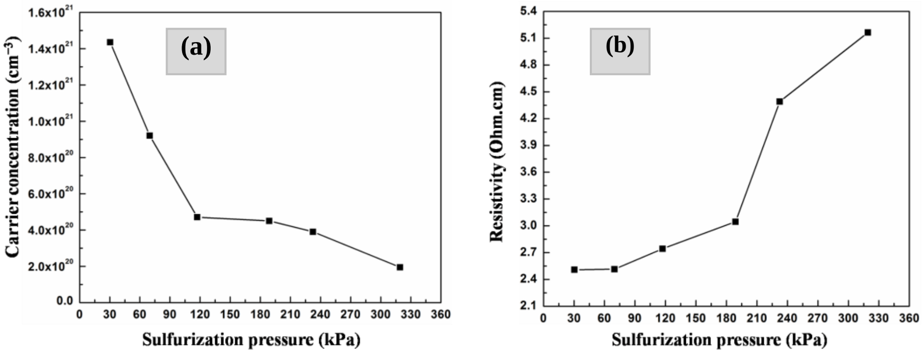

Fig. 8. AC field Hall effect measurement on the pyrite film at different sulfurization pressure (a) carrier concentration (b) resistivity

In order to confirm the type of conductivity the electrochemical Mott-Schottky measurement on the pyrite film was performed. The measurement was done on the film obtained at 319.2 kPa sulfurization pressure which is having the smallest charge carrier concentration in the present study. The measurement was done for 0.1 V to −0.4 V/SCE as this range corresponds to the stability region of the pyrite phase in dearerated aqueous solution of pH 6.5[45]. Representative plot of C^{-2} *vs.* voltage is shown in the Fig. 9. The positive slope of the curve confirms an n-type conductivity of the synthesized pyrite film.

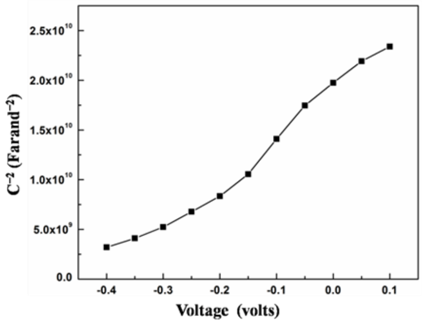

Fig. 9. Electrochemical measurement on the pyrite film obtained at 319.2 kPa sulfurization pressure

Fig.10(a) shows the absorption coefficient (α) as a function of incident photon energy for all the pyrite films. Its value is ~ 10^5 cm^{-1} for the photon energy > 1.40 eV ($\lambda < 885$ nm). The band gap can be obtained from the Tauc plot, that is, $(\alpha h\nu)^n$ vs. $h\nu$ plot where the symbols h, and α are Planck's constant, and absorption coefficient, respectively. Here the value of superscript n is considered to be 0.5 for the indirect band gap and 2 for the direct band gap. Representative Tauc plots corresponding to the pyrite films obtained at highest sulfurization pressures are shown in Fig. 10(b) and inset. The indirect band of 0.93 eV and direct band gap of 1.39 eV was found for the film obtained at 319.2 kPa sulfurization pressure. The indirect and direct band gap values extracted for all the pyrite films have been calculated. The indirect and direct band gap changed from 0.81eV to 0.93eV and 1.17eV to 1.39eV, respectively, with the increasing sulfurization pressure. Similar variation in the band gap with sulfurization pressure has been observed and attributed to the change in the density of defect-states present in the band gap [54].

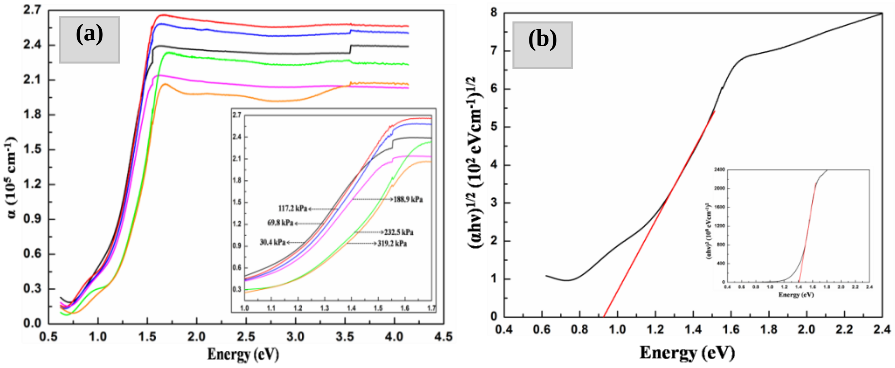

Fig. 10. (a) Absorption coefficient of the pyrite film at different sulfurization pressure (b) Indirect and direct band gap for pyrite films obtained at 319.2 kPa sulfurization pressure.

To check the photoactivity of the synthesized material the photocurrent measurement was performed. Fig.11 shows the photocurrent measurement performed at ambient temperature for the pyrite film synthesized at sulfurization pressure of 319.2 kPa. For these measurements silver contacts were placed on the two opposite edges of the film where the substrate was quartz. The current increased upon illuminating the films and dropped to a lower current value corresponding to dark condition (no illumination). The synthesized pyrite films showed a clear and stable phtoresponse.

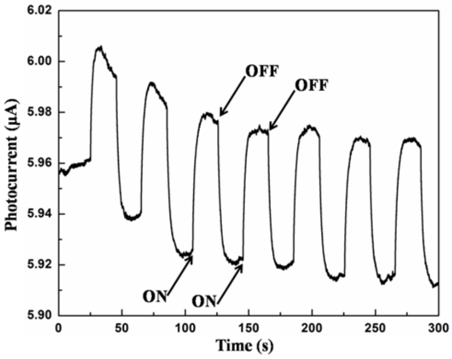

Fig. 11. Photocurrent measurement on the pyrite film obtained at 319.2 kPa sulfurization pressure.

4. Conclusions

Continuous, well adherent, and single-phase pyrite (FeS_2) films have been successfully obtained through the sulfurization of sol-gel synthesized hematite thin-films. The S/Fe ratio in these pyrite films approached the ideal value of 2 with the increasing sulfurization pressure. The reasons for the observed high sulfur vacancy concentrations even for those pyrite films obtained at sulfurization pressures higher than the atmospheric pressure are not clear. In this context, it is expected that by the end of sulfurization at 550 °C the pyrite films corresponding to each of the sulfurization pressures would have achieved certain stoichiometry. Whether this stoichiometry changes as the sulfur vapor pressure decreases during cool down stage, needs to be carefully investigated. This may also help in understanding the reason for high values of charge carrier concentration even though it decreased by an order of magnitude for the investigated pressure range. The charge carrier concentration needs to be further reduced to the workable level which would be suitable for PV application.

The electrical conductivity for the pyrite films has been found to be n-type which is in agreement with the recently reported works. This is contrary to the majority of reports that mention these films to be p-type. Few groups have even reported transition between p-type and n-type conductivity with the variation in synthesis temperature. These observations indicate that further investigations are required to understand and control the electrical properties of pyrite films.

Acknowledgements

The authors would like to acknowledge the financial support from the Department of Science and Technology (DST) India under the Solar Energy Research Initiative (SERI) program. The authors would also like to acknowledge the HMS Central Facility of IIT Bombay for the AC Field Hall effect measurement and Advanced Center for Materials Science (ACMS), IIT Kanpur for XRD, FESEM and XPS characterizations. The Central Glass Blowing Facility at IIT Kanpur has been very helpful with the customized calibration set-up made of quartz.

References

[1] G. Chatzitheodorou, S. Fiechter, R. Konenkamo, M. Kunst, W. Jaegermann, H. Tributsch, Mat. Res. Bull. **21**, 1481 (1986).
[2] M. C. Acevedo, M. S. Faber, Y. Tan, R. J. Hamers and S. Jin, Nano Lett.**12,** 1977 (2012).
[3] A. Ennaoui, S. Fiechter, G. Smestad, and H. Tributsch, First World Renewable Energy Congress, Reading, UK 458(1990).
[4] A. Ennaoui, H. Tributsch Solar Energy Materials **14,** 461 (1986).
[5] K. Buker, N. A. Vante and H. Tributsch, J. Appl. Phys.**72,**5721 (1992).
[6] M. Bronold, C. Pettenkofer and W. Jegermann, J. Appl. Phys. **76,** 5800 (1994).
[7] M. Limpinsel, N. Farhi, N. Berry, J. Lindemuth, C. L. Perkins, Q. Lin and Matt Law, Energy Environ. Sci. **7,**1974 (2014).
[8] P. A. Popov, P. P. Fedorov, S. V. Kuznetsov, Crystallogr. Rep. **58,** 319 (2013).
[9] M.-Y. Tsay, Y.-S. Huang, Y.-F.Chen, J. Appl. Phys. **74,**2786 (1993).
[10] G. Willeke, O. Blenk, C. Kloc, E. Bucher, J. Alloys Compd.**178**, 181 (1992).
[11] S. H. Chen, M. Y. Tsay, Y. S. Huang, J. T. Yu, J. Phys.: Condens. Matter **6,** 9211 (1994).
[12] A. L. Echarri, C. Sanchez, Solid State Commun. **15,** 827 (1974).
[13] T.-R. Yang, J.-T.Yu, J. Appl. Phys.**77,** 1710 (1995).
[14] K. P. Bhandari, P. J. Roland, T. Kinner, Y. Cao, H. Choi, S. Jeong, R. J. Ellingson, J. Mater. Chem.A **3,** 6853 (2015).
[15] G. Pementa, W. Kautek, Thin solid films**238,**213 (1994).
[16] C. D. L. Heras, C. Sanchez, Thin Solid Films **199,**259 (1991).
[17] G. Pimenta, W. Kautek, Thin Solid Films**219,**37 (1992).
[18] L. Huang, Y. Liu, L. Meng, J. Mater. Sci. Technol. **25,**237 (2009).
[19] M. Birkholz, D. Lichtenberger, C. Hopfner, S. Fiechter, Sol. Energy Mater. Sol. Cells **27,** 243 (1992).
[20] A. K. Raturi, L. Ndjeli, K. Rabah, Renewable Energy **11,** 191 (1997).
[21] P. Prabhukanthan, R. J. Soukup, N. J. Ianno, A. Sarkar, S. Kment, H. Kmentova,

C. A. Kamler, C. L. Exstrom, J. Olejnicek, S. A. Darveau, IEEE 2965 (2010).
[22] S. Nakamura, A. Yamamoto, Sol. Energy Mater. Sol. Cells **65,** 79 (2001).
[23] J. Oertel, K. Ellmer, W. Bohne, J. Rohrich, H. Tributsch, J. Cryst. Growth **198-199,** 1205 (1999).
[24] A. Yamamoto, M. Nakamura, A. Seki, E.L. Li, A. Hashimoto and S. Nakamura, Sol. Energy Mater.Sol. Cells **75,**451 (2003).
[25] J. M. LaForge, B. Gyenes, S. Xu, L. K. Hayens, L. V. Titova, F. A. Hegmann, M. J. Brett, Sol. Energy Mater.Sol. Cells**117,** 306 (2013).
[26] L. Samad, M. C. Acevedo, M. J. Shearer, K. Park, R. J. Hamers, S. Jin, Chem.Mater. **27,** 3108 (2015).
[27] D. Y. Wang, Y. Ting, C. C. Lin, S. S. Li, Y. T. Wang, C. C. Chen and C. W. Chen, Adv. Mater.**24,** 3415 (2012).
[28] B. Rezig, H. Dahman, M. Kenzari, Renewable Energy **2,** 125 (1992).
[29] S. Kment, H. Kmentova, A. Sarkar, R. J. Soukup, N. J. Ianno, D. Sekora, J. Olejnicek, P. Ksirova, J. Krysa, Z. Remes, Z. Hubicka, J. Alloys Compd.**607,** 169 (2014).
[30] Y. Bi, Y. Yuan, C. L. Exstrom, S. A. Darveau, J. Huang, Nano Lett. **11,** 4953 (2011).
[31] K. Sun, Z. Su, J. Yang, Z. Han, F. Liu, Y. Lai, J. Li and Y. Liu, Thin solid films **542,**123 (2013).
[32] J. R. Ares, I. J. Ferrer, F. Cuevas and C. R. Sanchez, Thin Solid Films**387,** 97 (2001).
[33] Y.H. Liu, L. Meng, L. Zhang, Thin Solid Films**479,** 83 (2005)
[34] L. Meng, Y. H. Liu, L. Tian, J. Cryst. Growth **253,** 530 (2003).
[35] L. Meng, J. P. Tu, M. S. Liu, Mater. Lett.**38** 103 (1999).
[36] G. Smestad, A. Ennaoui, S. Fiechter, H. Tributsch, W. K. Hofmann and M. Birkholz, Solar Energy Materials**20,** 149 (1990).
[37] R. J. Soukup, P. Prabhukanthan, N. J. Ianno, A. Sarkar, C. A. Kamler and D. G. Sekora, J. Vac. Sci. Technol. A**29,** 11001 (2011).
[38] A. Pascual, S. Yoda, M. Barawi, J. M. Clamagirand, J. R. Ares, I. J. Ferrer and C. Sanchez, J. of Phys. Chem. C **118,** 26440 (2014).
[39] R. Morrish, R. Silverstein and C. A. Wolden, J. Am. Chem. Soc.**134,** 17854 (2012).
[40] Y. Z. Dong, Y. F. Zheng, H. Duan, Y. F. Sun, Y. H. Chen, Mater. Lett.**59,** 2398 (2005).
[41] D. Wan, Y. Wang, B. Wang, C. Ma, H. Sun, L. Wei, J. Cryst. Growth**253,** 230 (2003).
[42] A. Gomes, J. R. Ares, I. J. Ferrer, M. I. da S. Pereira, C. Sanchez, Mater. Res. Bull. **38,** 1123 (2003)
[43] C. de I. Heras, I. J. Ferrer, C. Sanchez, J. Appl. Phys.**74,** 4551 (1993).
[44] L. Huang, F. Wang, Z. Luan, L. Meng, Materials Letters**64,** 2612 (2010).
[45] D. G. Moon, A. Cho, J. H. Park, S. H. Ahn, H. S. Kwon, Y. S. Cho and S. Ahn, Journal of Materials Chemistry A**2,** 17779 (2014).
[46] B. Ouertani, J. Ouerfelli, M. Saadoun, B. Bessais, M. Hajji, M. Kanzari, H. Ezzaouia, N. Hamadadou, J. C. Bernede, Mater. Lett.**59,**734 (2005).
[47] L. Meng, Y. H. Liu, L. Tian, Mater. Res. Bull.**38,** 941 (2003).
[48] D. Youzhong, Z. Yufeng, Z. Xiaogang, D. He, S. Yanfei, C. Yanhua, Science in China Ser. E Engineering and Materials Science**48,** 601 (2005).
[49] S. Kment, H. Kmentova, A. Sarkar, R. J. Soukup, N. J. Ianno, J. Krysa, Z. Hubicka, J. Olejnicek, C. L. Exstrom, S. A. Darveau, 37th IEEE Photovoltaic Specialists Conference (PVSC) (2011).
[50] F. Wang, L. Huang, Z. Luan, J. Huang, L. Meng, Mater. Chem. Phys. **132,** 505 (2012).
[51] X. Zhang, M. Manno, A. Baruth, M. Johnson, E. S. Aydil, C. Leighton, ACS Nano **7,** 2781 (2013).
[52] L. Meng, Y. H. Liu, W. Huang, Mater. Sci. Eng. B**90,**84 (2002).
[53] I. J. Ferrer, C. Sanchez, J. Appl. Phys.**70,** 2641 (1991).
[54] D. Wan, B. Wang, Y. Wang, H. Sun, R. Zhang, L. Wei, J. Cryst. Growth **257,**286 (2003).
[55] N. Berry, M. Cheng, C. L. Perkins, M. Limpinsel, J. C. Hemminger, M. Law, Adv. Energy Mater.**2,**1124 (2012).
[56] H. Rau, T. R. N. Kutty, J. R. F. G. De Carvalho, J. Chem. Thermodynamics**5,** 833 (1973).
[57] H. Rau, T. R. N. Kutty, J. R. F. G. De Carvalho, J. Chem. Thermodynamics**5,**291 (1973).
[58] C. D. L. Heras, G. Lifante,J. Appl. Phys. **82,** 5132 (1997).

[59] S. W. Lu, C. Harris, S. Walck, J. Mater. Sci.**44,** 541 (2009).
[60] R. Sun, M. K. Y. Chan, G. Ceder, Phys. Rev. B **83**, 235311 (2011).
[61] B. Yuan, W. Luan, S. Tu, Dalton Trans.**41,**772 (2012).
[62] W.L.Liu, X.H. Rui, H.T.Tan, C. Xu, Q. Y.Yan, H. H. Hng, RSC Adv. **4,** 48770 (2014).
[63] C. Wadia, Y. Wu, S. Gul, S. K. Volkman, J. Guo, A. P. Alivisatos, Chem. Mater. **21,** 2568 (2009).
[64] S. Seefeld, M. Limpinsel, Y. Liu, N. Farhi, A. Weber, Y. Zhang, N. Berry, Y. J. Kwon, C. L. Perkins, J. C. Hemminger, R. Wu, M. Law, J. Am. Chem. Soc.**135,**4412 (2013).
[65] X. Song, W. Shen, Z. Sun, C. Yang, P. Zhang and Lian Gao, Chemical Engineering Journal **290,**74 (2016).
[66] P. L. Gai, B. H. M. Billinge, A. M. Brown, Carbon **27,** 41 (1989).
[67] K. Ellmer, C. Hopfner, Philosophical Magazine **75,**1129 (1997).
[68] A. J. E. Rettie, H. C. Lee, L. G. Marshall, J. F. Lin, C. Capan, J. Lindemuth, J. S. McCloy, J. Zhou, A. J. Bard, C. B. Mulins, J. Am. Chem. Soc. **135,** 11389 (2013).
[69] J. R. Ares, M. Leon, N. M. Arozamena, J. S. Paramo, P Celis, I. J. Ferrer, C Sanchez, J. Phys.: Condens. Matter**10,** 4281 (1998).
[70] G. Willeke, R. Dasbach, B. Sailer, E. Bucher, Thin Solid Films**213,**271 (1992).
[71] S. C. Hsiao, K. W. Wu, S. H. Huang, S. H. Liu, S. H. Chiu, L. H. Chou, Appl. Phys Express **8,** 15201 (2015).
[72] A. Ennaoui, S. Fiechter, W. Jaegermann and H. Tributsch, J. Electrochem. Soc.: Electrochemical Science and Technology**133,** 97 (1986).